Depth Profiling the Near Surface of Polymer Films Using NEXAFS Spectroscopy

K.E. Sohn[1], M.D. Dimitriou[1], J. Genzer[2], D.A. Fischer [3],

C.J. Hawker[1,4], E.J. Kramer[1,5]

[1]Department of Materials, UCSB

[2] Department of Chemical and Biomolecular Engineering, NCSU

[3]National Institute of Standards and Technology

[4]Department of Chemistry and Biochemistry

[5]Department of Chemical Engineering, UCSB

December 1, 2008

Abstract

Depth profiling using near-edge X-ray absorption fine structure (NEXAFS) spectroscopy was used to determine the carbon atom density as a function of depth by analyzing the post-edge signal in NEXAFS spectra. We show that the common assumption in the analysis of NEXAFS data from polymer films, namely, that the carbon atom density is constant as a function of depth is not valid. This analysis method is then used to calculate the electron escape depth (EED) for NEXAFS in a model bilayer system that contains a perfluorinated polyether (PFPE) on top of a highly oriented pyrolitic graphite (HOPG) sample. Because the carbon atom densitites of both layers are known, in addition to the PFPE surface layer thickness, the EED is determined to be 1.95nm. This EED is

then used to measure the thickness of the perfluorinated surface layer of a poly(4-(1H, 1H, 2H, 2H-perfluorodecyl) oxymethylstyrene) (PFPS).

1 Introduction

Knowledge of surface composition of polymeric materials as well as organic self-assembled monolayers is necessary for many applications including anti-biofouling coatings for ships,[1–4] polymer field effect transitors[5–10] and polymer light emitting diodes (PLEDS),[11,12] and biomedical devices.[13–20] Near edge X-ray absorption fine structure (NEXAFS) spectroscopy and X-ray photoelectron spectroscopy (XPS) are often employed to determine the composition in the near surface region of a sample.[21–27] The two techniques are similar, but have distinct differences. However, when used in tandem, they provide valuable information about the surface.

NEXAFS spectroscopy uses tunable, polarized X-rays from a synchrotron source to determine which bonds are present within the top 2nm of the surface as well as their orientation.[3,28,29] The X-rays used in NEXAFS spectroscopy excite a core electron into an empty molecular orbital, leaving a hole in the core shell. This hole is filled by an electron from a higher energy level, and an Auger electron is emitted. The number of Auger electrons that are detected for a given X-ray energy supplies information about the number of core-holes that are created, and therefore the transitions that are occuring. Because NEXAFS spectroscopy is focused on orbitals instead of individual elements, it is possible to differentiate between a $C-C$ and $C=C$ bond due to the presence of the π orbital in the double bond, a capability that XPS does not have.

The typical experimental geometry for NEXAFS is shown in Figure 1, which depicts the tunable soft X-ray beam, the goniometer on which the sample is

mounted and the partial electron yield detector that detects the Auger photoelectrons. The goniometer can be rotated so that the incident X-ray beam makes an angle θ with respect to the sample surface. There are two possible methods for depth profiling using NEXAFS spectroscopy. The first is to vary the negative bias on the entrance grid in front of the partial electron yield (PEY) detector. The purpose of this grid is to screen out electrons that have lost a significant amount of energy while leaving the sample. As the bias becomes more negative, more electrons that have lost energy are prevented from reaching the detector, increasing the surface sensitivity.[30] Another way to depth profile is to vary ϕ, the electron emission angle from the sample normal, just as in XPS (See Figure 1). However, because NEXAFS spectroscopy is sensitive to bond orientation, there are two factors that cause the intensity to vary as a function of ϕ (and θ): the orientation of a particular bond and the depth of the bond below the surface of the film. These two effects need to be separated in order to successfully use NEXAFS spectroscopy as a depth profiling technique.

In addition, the sampling depth, the electron escape depth (EED), of the technique must be known. Genzer et al. have experimentally determined the EED for NEXAFS at two values of θ's where the effects of orientation should be the same for different values of ϕ, but these results relied on very small signals from methylene groups under a fluorinated self-assembled monolayer (SAM). The possibility that the surface of the semifluorinated SAM might have been contaminated by airborne hydrocarbons or siloxanes (common in laboratory environments containing pumps) was not considered.[30] Krishnan et al. have calculated the inelastic mean free path (IMFP) for polymeric systems using a method developed by Cumpson, but did not verify it experimentally.[3,31] The IMFP is a measure of the average distance an electron can travel through a material without being inelastically scattered, and therefore losing energy, since

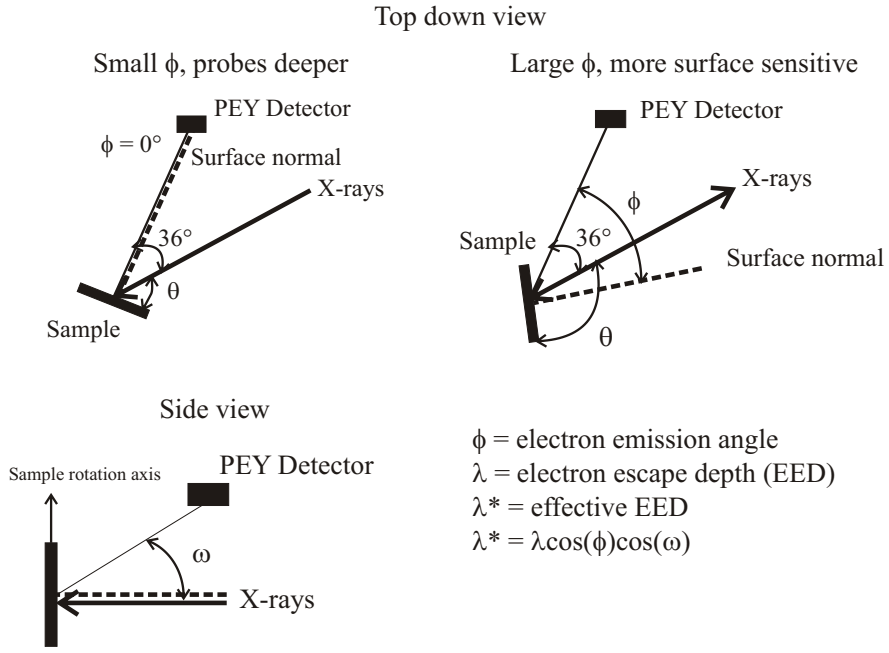

Figure 1: Depth profiling with NEXAFS spectroscopy. The sample is rotated with respect to the X-ray beam to change the effective electron escape depth, λ^*. The angle between the PEY detector and the incident X-rays is fixed.

the probability of inelastic scattering after traveling a distance x is given by $e^{-x/IMFP}$.

In XPS since the energy of the photoelectron is measured accurately, the IMFP can be used directly to compute the photoelectron yield for a given depth profile as a function of ϕ. In NEXAFS since the EGB does not discriminate Auger electrons that have lost a small amount of energy from those that have lost none, the electron escape depth (EED) will be larger than the IMFP for the Auger electron energy ($\sim$ 263eV for carbon atoms) and it will increase with decreasing negative EGB.[30]

In the case of a geometry where the electron detector is not in the same plane as the sample normal and the incoming X-rays, another angle, ω, must be taken into account. This is the angle that the electron detector makes with the plane defined by the incoming X-ray beam and the sample normal (See Figure 1). In this case the effective EED will be $\lambda^* = \lambda cos(\phi)cos(\omega)$.

In order to determine the EED for NEXAFS, a model system of highly oriented pyrolytic graphite (HOPG) with a thin surface layer of perfluoropolyether (PFPE) has been used. The PFPE layer is Fomblin Z-03 and has the formula CF_3-[(O-CF_2-CF_2)$_m$-(O-CF_2)$_n$]-O-CF_3 where $m + n$ varies between $40 - 180$ and m/n ranges from $0.5 - 2$. This system was chosen because the HOPG has π bonds with a known orientation, while the PFPE has no π bonds. Additionally important is that the exact thickness of the PFPE layer can be independently determined using other characterization methods.[32]

The other important aspect of this work is the development of an analysis method using the post-edge data to accurately depth profile through different types of samples. By fitting the post-edge data prior to normalization, the effects of non-uniform carbon atom density with depth, as well as surface layer thicknesses, can be determined. Previous work attempting to depth profile using NEXAFS spectroscopy assumed a constant density as a function of depth, but our work reported below shows that the changing carbon atom density must be taken into consideration, and that, in addition, this information provides useful data to constrain models of the polymer surface.[3,30]

2 Theory

At normal X-ray incidence, the number of Auger electrons generated from a slice dz below the surface is

$$N_e dz = I_0 A_0 \mu_E dz \tag{1}$$

where μ_E is the X-ray energy dependent absorption coefficient giving rise to the Auger electrons, A_0 is the area irradiated by the incident X-rays and I_0 is the incident photon flux density.[28] I_0A_0 is constant as the sample is tilted because the intensity per unit area decreases by the same factor that the irradiated area increases as the sample tilts to more glancing angles, i.e. theta decreases. The effective absorption coefficient, $\mu_{effective}$, is not constant, however, as θ is varied:

$$\mu_{effective} = \frac{\mu_E}{sin(\theta)} \tag{2}$$

because the length of the path traveled by a photon through a thickness dz of material is dz/sin(θ). When $\theta \neq 90°$, Equation 1 becomes

$$N_e dz = \frac{I_0 A_0 \mu_E dz}{sin(\theta)} \tag{3}$$

and describes the number of Auger electrons created in a slab dz within the sample. In writing Equation 3 the decrease in X-ray intensity with depth ($I(z) = I_0 e^{-\frac{-\mu_E(z)}{sin(\theta)}}$) is neglected, since experimentally the X-ray absorption legnth, $\frac{1}{\mu_E}$, is much greater than the Auger electron EED.[28] The absorption coefficient is related to the energy-dependent absorption cross section by:

$$\mu_E = n_v(z)\sigma_E \tag{4}$$

where $n_v(z)$ is the number density of carbon atoms capable of undergoing the transition described by σ_E. The number density of carbon atoms is determined by:

$$n_v(z) = \frac{\rho_m(z) N_{Av}}{M} \tag{5}$$

where N_{Av} is Avogadro's number, ρ_m is the mass density of carbon atoms, and M is the atomic mass, i.e. 12 for carbon. By integrating Equation 1, the number of Auger electrons created throughout the sampling depth can be determined:

$$I = \frac{\Omega}{4\pi} \int_0^\infty dz N_e = \frac{I_0 A_0 \Omega}{4\pi sin(\theta)} \int_0^\infty dz n_v(z) \sigma_E e^{-\frac{z}{\lambda cos(\phi) cos(\omega)}} \tag{6}$$

where Ω is the solid angle subtended by the electron detector.

2.1 Post-edge Intensity Analysis

In general, the absorption cross section, in addition to depending on energy, depends on the angle δ between the vector matrix element, or transition dipole moment (TDM) of the final orbital state of the excited atom and the electric field vector of the X-ray beam. For σ^* final states, the TDM points along the bond axis, but for π^* final states the TDM points in the same direction as the p-component of the final state orbital. For the transitions to these states

$$\sigma_E = \sigma(h\nu) cos^2(\delta) \tag{7}$$

where $h\nu$ is the X-ray energy. At energies far above the absorption edge and any π^* or σ^* final state, the photoelectron is ejected into the continuum and any dependence on the directionality of the molecular orbitals is lost such that

$$\sigma_E = \sigma_{cont}(h\nu) \tag{8}$$

At a 390eV X-ray energy, well above the absorption edge, Equation 6 can be simplified

$$I_{390} = \frac{\Omega}{4\pi}\frac{I_0 A_0}{sin(\theta)}\sigma_{cont}(390eV)\int_0^\infty n_v(z)e^{-\frac{z}{\lambda cos(\phi)cos(\omega)}} \tag{9}$$

since all carbon atoms contribute to the photoelectrons being ejected into the continuum. In addition if $n_v(z)$ is constant as a function of depth

$$I_{390} = \frac{\Omega}{4\pi}\frac{I_0 A_0}{sin(\theta)}\sigma_{cont}(390eV)n_v cos(\phi)cos(\omega)\lambda \tag{10}$$

and for such a sample a plot of $\frac{I_{390}}{I_0}\frac{sin(\theta)}{cos(\omega)}$ versus $\cos(\phi)$ must yield a straight line through the origin with a slope of $\frac{\Omega}{4\pi}A_0\sigma_{cont}(390eV)n_v$. Let us now suppose there is a layer of thickness t of material with a carbon atom number density, $n_{v,1}$ (i.e. PFPE) on a thick substrate (i.e. highly oriented pyrolytic graphite) with a carbon atom density, $n_{v,2}$. Integrating Equation 9 yields:

$$I_{390} = \frac{\Omega}{4\pi}\frac{I_0 A_0}{sin(\theta)}\lambda cos(\phi)cos(\omega)\sigma_{cont}(390eV)n_{v,2}[(1-\frac{n_{v,1}}{n_{v,2}})e^{-\frac{t}{\lambda cos(\phi)cos(\omega)}}+\frac{n_{v,1}}{n_{v,2}}] \tag{11}$$

In principle, dividing the intensity from the layered sample by that from the bare one should allow a determination of λ. Even if there is a very thin layer of contamination on the "bare" substrate, which is very difficult to avoid given the conditions surrounding the beamline at a storage ring with its many pumps, fitting data on a plot $\frac{I_{390}}{I_0}\frac{sin(\theta)}{cos(\omega)}$ versus $\cos(\phi)$ should allow one to extract values for $n_{v,1}$ and $\frac{t}{\lambda}$ for the contaminated substrate and thus the correct values for (Equation 10) for the truly uncontaminated sample. If $\frac{t}{\lambda cos(\phi)cos(\omega)} \ll 1$ as would be the case where $\frac{t}{\lambda}$ is small and $\cos(\phi)$ is close to 1 we can expand the

exponential in Equation 11 to yield:

$$I_{390} = \frac{\Omega}{4\pi}\frac{I_0 A_0}{sin(\theta)}\lambda cos(\omega)\sigma_{cont}(390eV)[n_{v,2}cos(\phi) - \frac{(n_{v,2} - n_{v,1})t}{\lambda cos(\omega)} + ...] \quad (12)$$

A plot of $\frac{I_{390}}{I_0}\frac{sin(\theta)}{cos(\omega)}$ versus cos(ϕ) would thus have the same slope as for the bare interface but with a negative intercept. In the limit when $\lambda cos(\phi)cos(\omega) \ll t$:

$$I_{390} = \frac{\Omega}{4\pi}\frac{I_0 A_0}{sin(\theta)}\lambda cos(\omega)\sigma_{cont}(390eV)n_{v,1}cos(\phi) \quad (13)$$

the result is the same as for a film of carbon atom number density $n_{v,1}$ of infinite thickness. Thus if $n_{v,1} \ll n_{v,2}$ the slope of the plot of $\frac{I_{390}}{I_0}\frac{sin(\theta)}{cos(\omega)}$ versus cos(ϕ) will tend toward the one predicted by Equation 13 for small cos(ϕ), giving important information on the carbon atom number density as a function of depth.

2.2 Order Parameter Calculation

By varying the angle between the TDM for a given orbital transition and the electric field vector of the polarized X-rays, the orientational order parameter, S, of the TDM can be determined. When the electric field vector is parallel to the TDM, a maximum in peak intensity for that bond is detected. The TDM for a σ bonded carbon atom lies along the bond axis, while the TDM for a π bonded carbon atom is perpendicular to the bond axis and parallel to the p orbitals that combine to form the π orbital.[28]

If it is assumed that the film is isotropic within the plane of the film, the usual condition for polymer films cast and/or annealed on a substrate, the average orientation for a given bond is determined using the three molecular orientation

factors:

$$f_z = \int \{cos^2(\alpha)[f(\alpha)]\} d\Omega \tag{14}$$

where dΩ is the differential solid angle, α is the angle between the surface normal, **z**, and the TDM for the given bond, and f(α) is the TDM distribution function of the orbital.[29,30] It follows from the in-plane isotropy assumption that

$$f_x = f_y = \frac{1 - f_z}{2} \tag{15}$$

where z is normal to the film surface and x and y are orthogonal axes in the film surface.[29] If the probability, $f(\alpha)$, that a given TDM is at an angle α is normalized so that

$$\int f(\alpha) = 1 \tag{16}$$

and

$$f_x + f_y + f_z = 1, \tag{17}$$

the order parameter, S, for the TDM can be determined using:

$$S = \frac{1}{2}(3f_z - 1) \tag{18}$$

where $S = 1$ means that the TDM of the bonds are completely oriented with the z direction and $S = -\frac{1}{2}$ means that the TDM of the bonds are oriented in the plane of the film.[29,33]

The NEXAFS spectra need to be normalized for comparison of data at multiple angles and between samples. This is done by first dividing the data by an I_0 value determined by measuring the electrons emitted from a gold grid in the beam after the monochromator to obtain the partial electron yield (PEY). This procedure is necessary both because the beam current in the storage ring

is decreasing slowly over time, decreasing the intensity of the peaks for each transition and because the beam intensity after the monochromator varies with energy. The next step usually is to do a pre-edge background subtraction so that the baseline is zero, followed by a post-edge normalization. This post-edge normalization ensures that the same number of carbon atoms are being considered in each spectrum. If the number density of carbon atoms, n_v, is constant from the film surface throughout the depth of the sample, the post edge intensity may be arbitrarily scaled to 1.

However, if the number density of carbon atoms changes as a function of depth, another normalization procedure is required, as is the case with the model system used here. The data for the PFPE/HOPG are normalized by dividing by the intensity of bare HOPG at 390eV for each angle. The data for the "bare" HOPG shown later indicate that there is a small layer of contamination on the HOPG, but it is possible to determine the values for HOPG without contamination using Equation 11, and these are the values used for the post-edge normalization. This normalization method accounts for the difference in n_v between the PFPE and HOPG. The energy at which the normalization was done was chosen here to be 390eV since this is above the very strong EXAFS oscillations from the HOPG that arise from backscattering of the emitted photoelectrons from nearest and next-nearest neighbor carbon atoms.

Whether or not the π or σ bonds are oriented, the post-edge normalized intensity for a sample with uniform carbon number density as a function of depth will have the form:

$$I = A + Bcos^2(\theta) \tag{19}$$

for a given transition where A and B are constants.[3,28,29] These constants can be used to determine the orientational order parameter for a given TDM:

$$S = -\frac{B}{3AP + B} \tag{20}$$

where P is the polarization of the X-rays (0.85 for beamline U7A at the NSLS).[29,30,33] Stöhr and Samant have shown that

$$f_z = \frac{AP + B}{PI_{tot}} \tag{21}$$

where I_{tot} is the total integrated intensity.[29] From the orientational order parameter defined in Equation 18, substitution and rearrangement yield:

$$A = \frac{1}{3}(1 - S)I_{tot} \tag{22}$$

$$B = SPI_{tot} \tag{23}$$

Substituting these values for A and B into Equation 19 yields:

$$I = I_{tot}(\frac{1}{3} - \frac{S}{3} + SP\cos^2(\theta)) \tag{24}$$

Substituting these values into Equation 6 results in the non post-edge normalized intensity throughout the depth of the film for a given transition:

$$I = \frac{\Omega}{4\pi}\frac{I_0 A_0}{sin(\theta)}\int_0^\infty dz n_v(z)\sigma(h\nu)(\frac{1}{3} - \frac{S(z)}{3} + S(z)P\cos^2(\theta))e^{\frac{-z}{\lambda cos(\phi)cos(\omega)}} \tag{25}$$

where S(z) is the depth dependent order parameter and λ is the EED.[3] The term $n_v(z)$ enters into the equation to account for any variation in the fraction of carbon atoms associated with the transition and the total carbon atom number density throughout the depth of the sample.

3 Experimental

Preparation of PFPE films on HOPG. Fomblin Z-03, with a molecular weight of 4kg/mol, was supplied by Solvay Solexis and used as received. Thin films were dip coated onto HOPG using dilute solutions, 0.04wt%-0.16wt%, of PFPE in perfluorohexane (Aldrich). Films were dip coated at a rate of 10mm/min using the dip coating motor from a NIMA Langmuir-Blodgett trough (Coventry, UK). The film thickness was measured using XRR and ellipsometry by a method similar to Toney et al.[32] To prevent hydrocarbon contamination from the atmosphere as much as possible, samples were stored under high vacuum until characterization.

Preparation of 4-(1H,1H,2H,2H-Perfluorodecyl) oxymethylstyrene. 1H, 1H, 2H, 2H-perfluorodecanol (97%) and 4-chloromethylstyrene (90%) were purchased from Aldrich and used without further purification. Synthesis was performed as reported in the literature.[34] A mixture of 4.6g (10 mmol) of 1H,1H,2H,2H-Perfluorodecanol and 40mL of 50 wt% aqueous NaOH solution was vigorously stirred at 80°C for one hour. 0.5g (1.5 mmol) of tetrabutylammonium hydrogensulfate (TBAH) in 40mL of dichloromethane was added. This was followed with the dropwise addition of 3.25g (21 mmol) of 4-chloromethylstyrene to the suspension. The mixture was stirred at 40°C for 15 hours. The organic layer was separated, washed with water, and dried over $MgSO_4$. The solvent was evaporated yielding an oily residue that was purified by double elution on silica gel, once with hexane-dichloromethane (9/1 v/v) and once with hexane-ethyl acetate (30/1) as the eluent. 1.4g of pure 4-(1H,1H,2H,2H-perfluorodecyl)oxymethylstyrene (24% yield) as a white powder was obtained. 1H-NMR (CDCl3): 7.2-7.5 (m, Ar, 4H), 6.7 (dd, CH_2CHPh, 1H), 5.7 and 5.2 (CH_2CHPh, 2H), 4.5 (s, $PhCH_2O$, 2H), 3.8 (t, OCH_2CH_2, 2H), 2.5 (tt,

$CH_2CH_2CF_2$, 2H).

Preparation of poly(4-(1H, 1H, 2H, 2H-perfluorodecyl) oxymethylstyrene). 0.5g (860 mol) of 4-(1H, 1H, 2H, 2H-perfluorodecyl) oxymethylstyrene and 1.7mg (10 mol) of azobisisobutyronitrile were dissolved into 1mL of trifluorotoluene in a 5mL ampule with a magnetic stir bar. The mixture was freeze-pump-thawed three times and sealed under vacuum. Free radical polymerization was then carried out at 70°C for 48 hours. The polymer was then retrieved via double precipitation in methanol and dried under vacuum. 0.22g of poly(4-(1H,1H,2H,2H-perfluorodecyl)oxymethylstyrene) (44% yield) was obtained. Figure 2 shows the chemical structure of the polymer.

Ellipsometry Measurements. The thickness of the PFPE layer was determined using a Beaglehole Instruments Picometer Ellipsometer (Wellington, New Zealand) with a HeNe laser (λ = 632.8nm) that works based on phase modulation.[35,36] The value of the refractive index used for Fomblin Z-03 is the bulk value, n=1.3.[32] The thickness of the PFPE layer was determined using a previously published method.[36]

XPS Characterization. XPS measurements were performed using a Kratos Axis Ultra (Manchester, UK) with monochromated aluminum K_α radiation at 1486.6eV. Low energy electrons were injected from a filament to provide charge compensation to the sample. Spectra were collected at 225W with a 40eV analyzer pass energy. Three scans were taken for each sample with 0.05eV resolution and a dwell time of 300ms. The samples can be rotated with respect to the electron energy analyzer to change the electron emission angle and change the sampling depth of the film.[34]

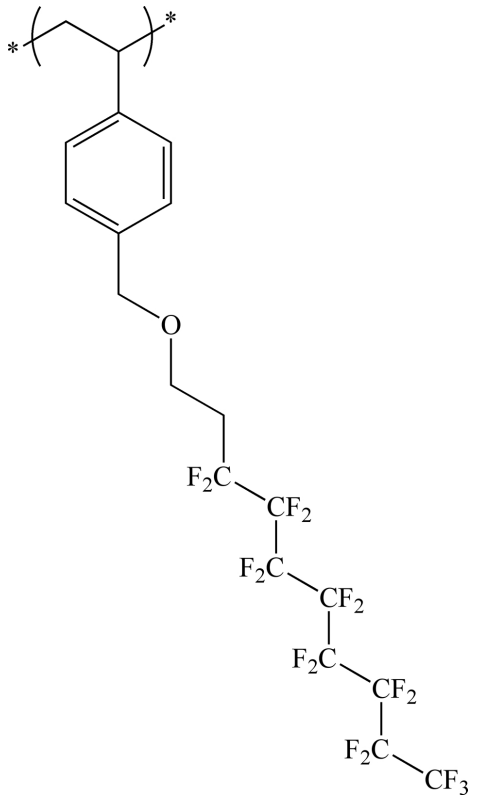

Figure 2: Chemical structure of perfluoroalkyl functionalized polystyrene.

NEXAFS Spectroscopy Measurements NEXAFS spectroscopy was performed at the NIST/Dow endstation of beamline U7A at the National Synchrotron Light Source at Brookhaven National Laboratory. The endstation has a goniometer that varies the orientation of the sample with respect to the incoming X-rays. The partial electron yield (PEY) was recorded with a channeltron electron multiplier with a variable entrance grid bias (EGB). For all measurments reported below, the EGB was set to -150V.

4 Results and Discussion

4.1 Determination of the Electron Escape Depth

Variable angle ellipsometry was used to measure the thickness of the PFPE layers on HOPG. The thicknesses of the PFPE samples reported here are 0.88 and 0.9nm. X-ray photoelectron spectroscopy (XPS) was used to confirm the presence of the PFPS on the HOPG after dipcoating. The XPS spectra showed peaks at the expected binding energies, which correspond to the bonds present in the PFPE. Representative spectra are shown in the Supporting Information.

NEXAFS spectra were recorded at the carbon K-edge over a large angular range, $20^\circ < \theta < 125^\circ$ and were normalized by the intensity of the incoming X-ray beam, I_0. A linear background was then subtracted based on the slope of the pre-edge region. Since the background and this slope also according to theory scale as $\cos(\phi)/\sin(\theta)$, we find the best straight line fit to a plot of background slope versus $\cos(\phi)/\sin(\theta)$ that passes through the origin and then use the best fit slopes at each angle to subtract the background. Due to the difference in carbon atom density between the HOPG substrate and the surface layers, no post-edge normalization has been performed. Figure 3 shows the HOPG spectra after division by I_0 and the background subtraction. Figure 4

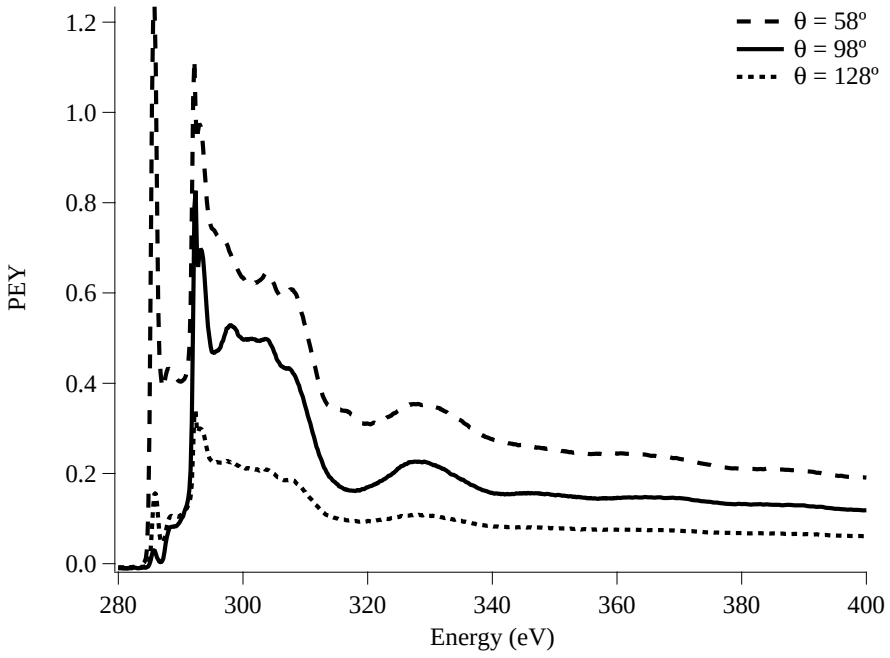

Figure 3: Selected NEXAFS spectra for bare HOPG after background subtraction. Spectra were taken in 10 degree intervals from $\theta = 28° - 98°$ and 5 degree intervals from $\theta = 98° - 128°$.

shows the PFPE/HOPG data after the same treatment.

The post-edge intensities provide information about the concentration of carbon atoms within the sampling depth of the film. Figure 5 shows the intensity at 390eV for the "bare" HOPG, the PFPE coated HOPG and the hypothetical intensity for clean HOPG as a function of $\cos(\phi)$. The data for the PFPE coated HOPG for $\cos(\phi)$ close to 1 can be fitted with a straight line with a negative intercept as expected from Equation 12. From the mass densities of PFPE and HOPG a value of $y = \frac{n_{v,1}}{n_{v,2}} = 0.16$ was determined and using Equation 11 h, where $h = \frac{t}{\lambda cos(\omega)}$, was varied to produce the best fit to the data. The values of h = 0.51, of the 0.88nm thick PFPE film and h = 0.61 for the 0.9nm thick PFPE

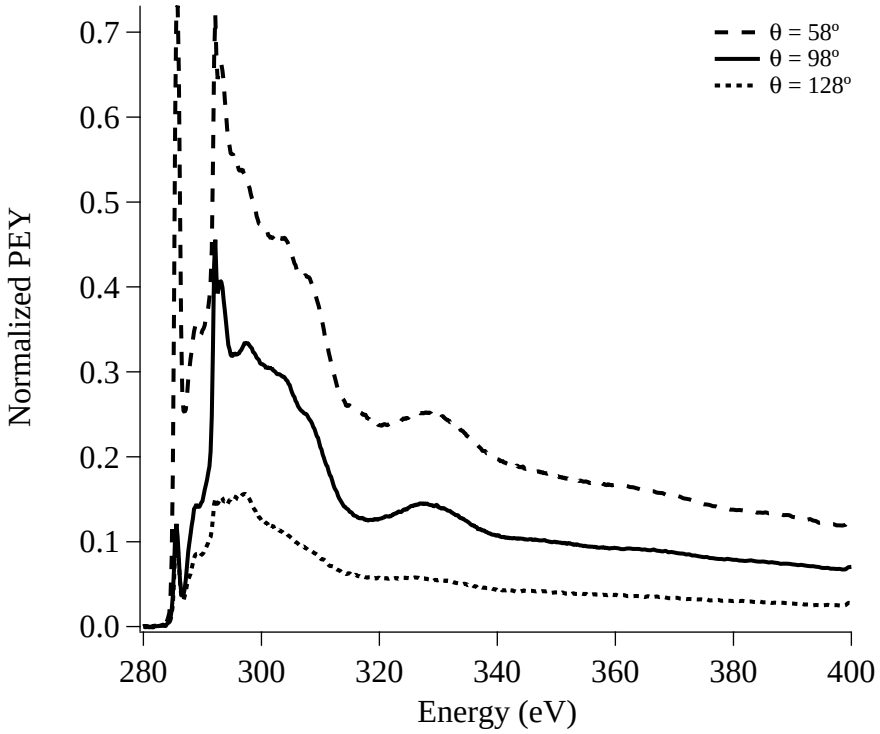

Figure 4: Selected NEXAFS spectra for PFPE coated HOPG after background subtraction. Spectra were taken in 10 degree intervals from $\theta = 28^\circ - 98^\circ$ and 5 degree intervals from $\theta = 98^\circ - 128^\circ$.

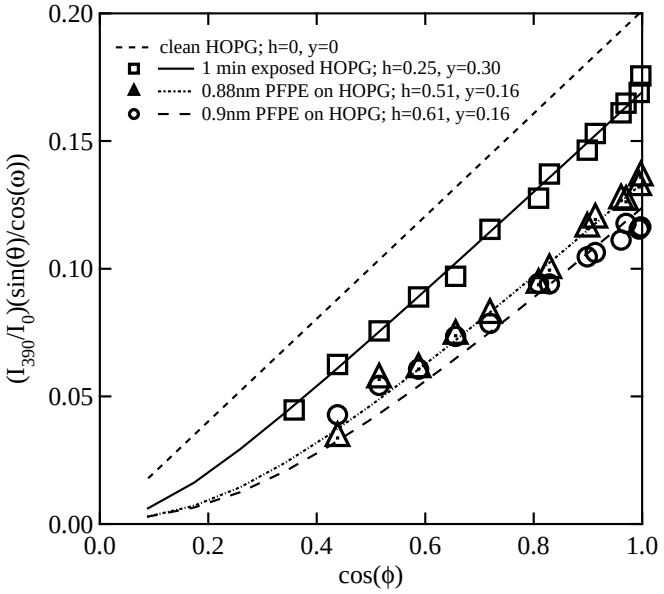

Figure 5: Intensity at 390eV after background subtraction for clean HOPG, "bare" HOPG and a 0.88nm thick PFPE film on HOPG. A 0.44nm thick layer of contamination containing carbon atoms is responsible for the offset in the HOPG data.

film, determined by ellipsometry, were used to determine a value of the EED of $\lambda = 1.95 \pm 0.15$nm. This value of the EED can be compared with an estimated value for the IMFP of 0.6nm for an electron with a kinetic energy of 263eV in a PFPE material using the method developed by Cumpson, which is reasonable considering the previously mentioned fact that the channeltron detector, with an EGB = -150V, does not discriminate between Auger electrons that have lost less than -113eV due to inelastic scattering and those that have not.[3,30,31]

However it is clear from Figure 5 that the bare HOPG, which was exposed to the air at the NSLS for about 1 minute between the time the surface was prepared by cleaving and the time it was loaded into the vacuum chamber, also has a layer of material containing a lower carbon atom density on the HOPG.

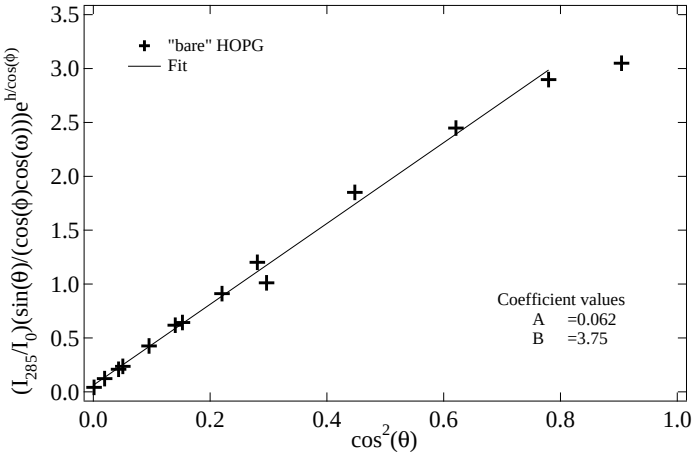

Figure 6: Intensity of the C 1s $\rightarrow \pi^*_{C=C}$ transition, which is used to determine the order parameter, $S_{C=C} = 0.959$.

Other experiments in which the HOPG was exposed to the air of the NSLS for longer times show an increase in the amount of contamination. Fitting the data to Equation 11 results in a best fit (solid line) with $y = 0.3$ and $h = 0.25$. The contamination layer has a lower carbon atom density (typical for hydrocarbons) than the PFPE and a thickness of about 0.5nm. Note also that the clean HOPG line can be closely approximated by a line with the initial slope of the "bare" HOPG that passes through the origin of Figure 5, as expected from Equation 12.

In order to determine the order parameter for a given transition, the intensity of the peaks for that transition must be treated in a similar way to the post-edge intensities. Equation 26 gives the intensity for the C 1s $\rightarrow \pi^*_{C=C}$ transition:

$$\frac{I}{I_0}\frac{sin(\theta)}{cos(\omega)cos(\phi)}e^{\frac{t}{\lambda cos(\omega)cos(\phi)}} = \frac{\Omega A_0}{4\pi}\lambda n_{\pi^*_2}\sigma_{\pi^*}(\frac{1}{3} - \frac{S_{\pi^*}}{3} + S_{\pi^*}Pcos^2(\theta)) \quad (26)$$

Figure 6 shows the left side of Equation 26 as a function of $\cos^2(\theta)$. The

main difference between these data and those shown for the post-edge is that these data only take into account carbon atoms that have π bonds, whereas the post-edge data represent all of the carbon atoms within the sampling depth. The post-edge data show that there is a thin contamination layer that will attenuate the signal for the C 1s $\rightarrow \pi^*_{C=C}$ transition from the HOPG, and this is accounted for by adding in an exponential term, $e^{\frac{h}{cos(\phi)}}$, where h is the same as that used to fit the post-edge data. Fitting a line to these data, where A is the intercept of the fit and B is the slope, allows one to determine the order parameter for the transition using Equation 20. Using the fit parameters, an order parameter of $S_{C=C} = 0.959$ is calculated, which is close to the expected order parameter of $S_{C=C} = 1$ for perfectly oriented HOPG. If the contamination contains any $C = C$ bonds, they will contribute to the signal, but will almost certainly not have the same orientation of the HOPG, and can be the cause of the slightly decreased order parameter.[32] The order parameter for the C 1s $\rightarrow \pi^*_{C=C}$ transition can also be calculated for the PFPE on HOPG sample. The only difference is that there is a thicker layer attenuating the sample, due to the PFPE layer. Figure 7 shows the data for the C 1s $\rightarrow \pi^*_{C=C}$ transition as a function of $\cos^2(\theta)$; the order parameter is $S_{C=C} = 0.68$, indicating that there is contamination on the sample that contain $C = C$ bonds, which are decreasing the order parameter from the expected value of 1 for HOPG.

4.2 Measurement of a Fluorinated Surface Layer in a Homopolymer Film

A model system for depth profiling with NEXAFS is a polystyrene homopolymer with perfluoroalkyl side chains linked at the para position of the phenyl ring by an ether bond and a methylene group (PFPS). Due to the lower surface energy of the PFPS side chains, these are expected to segregate to the surface,

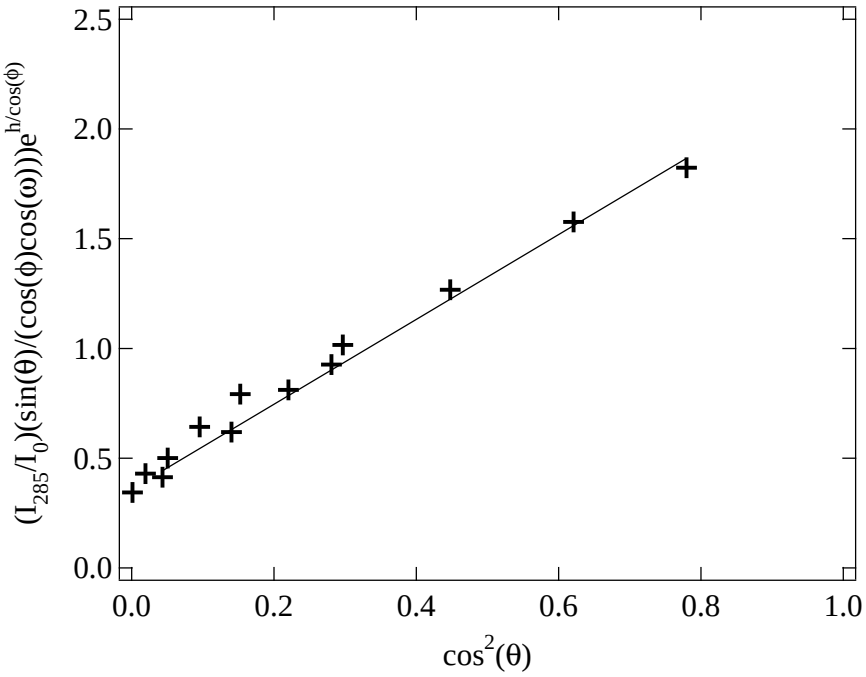

Figure 7: Intensity of the C 1s $\rightarrow \pi^*_{C=C}$ transition for the 0.88nm PFPE on HOPG. The order parameter is $S_{C=C} = 0.68$.

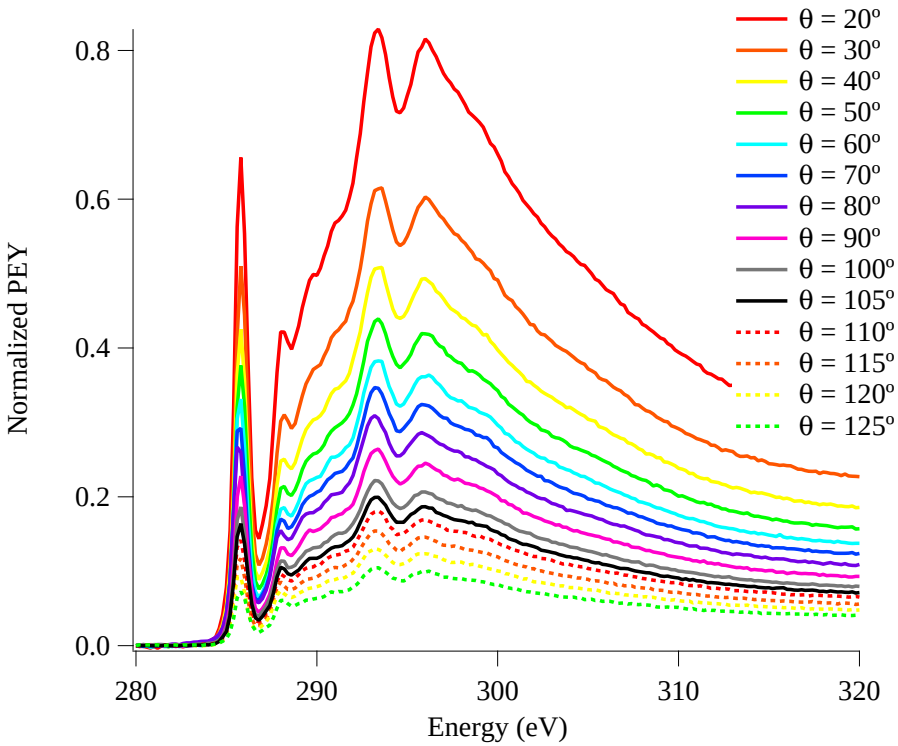

Figure 8: NEXAFS spectra for PFPS at various incident X-ray angles after pre-edge subtraction.

producing a thin surface layer enriched with perfluoroalkyl bonds. Analysis of the post-edge intensities allows for determination of the thickness of this layer.

Figure 8 shows spectra for the PFPS after the pre-edge baseline subtraction. The thickness of the perfluorinated surface layer can be determined using the same fitting method as was used to determine the thickness of the contaminated layer on the HOPG. Figure 9 shows a plot of $\frac{I_{320}}{I_0}\frac{sin(\theta)}{cos(\omega)}$ vs cos(ϕ), where the dashed line represents the predicted values for a polystyrene homopolymer. For the carbon density of the side chains, the value determined by Starkweather for amorphous polytetrafluoroethylene (PTFE) was used and the density of polystyrene was used for the underlayer.[37] Using the density of PS is not exact,

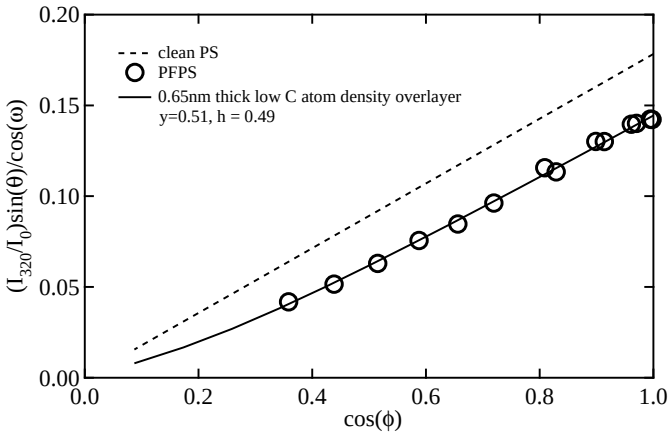

Figure 9: Intensity of the PEY signal at 320eV after background subtraction. Fitting the data shows that the low carbon atom density surface layer is 0.64nm thick.

because there will be some side chains from buried polymer chains that will change the carbon density. Using these values for the carbon atom densities, a thickness of 0.78nm was determined for the side-chain rich surface layer. It should be noted that this layer thickness just corresponds to the layer of lower density, and probably includes some of the phenyl rings.

Figure 10 shows the data from the C 1s $\rightarrow \pi^*_{C=C}$ transition and calculated values for "clean" polystyrene as a function of $\cos(\phi)$. Fitting the data yields a value of $h = 0.28$, which corresponds to a layer thickness of 0.45nm. This differs from the thickness of the fluorinated layer determined from the post-edge data because that overlayer probably contains some of the phenyl rings, whereas the layer measured here is the layer covering the phenyl rings. It makes sense that the overlayer thickness determined here is less than that determined from the data at 320eV. However there is an additional layer of contamination on the surface of the sample that can be inferred from the results shown in Figure 11.

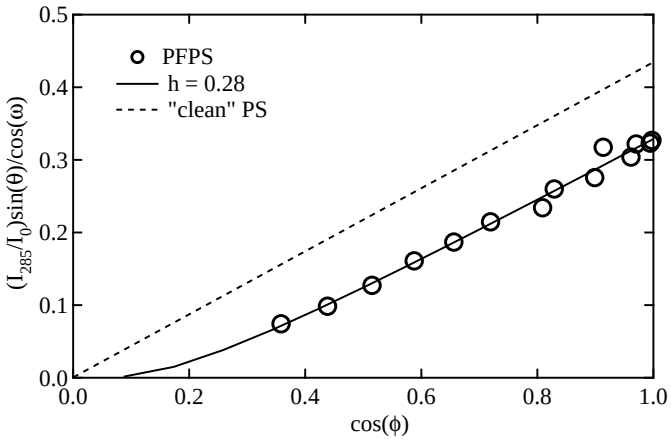

Figure 10: Intensity of the C 1s $\rightarrow \pi^*_{C=C}$ transition for the PFPS and clean polystyrene.

Figure 11 shows the data for the intensity of the C 1s $\rightarrow \sigma^*_{C-F}$ transition as a function of $\cos(\phi)$. If the side chains were truly at the surface, the data should fit on a line that extrapolates to zero, however it is clear that this is not the case, indicating that there is some contamination on the surface that attenuates the signal. In order for the data shown in Figure 11 to fit on a line that passes through the origin, an exponential term accounting for the attenuation of the signal with $h = 0.19$ was required, corresponding to an overlayer thickness of 0.30nm. It is unexpected that this contamination would be present for a sample with a low surface energy, but it is clear from the data that it is there. The most likely source of this contamination is from hydrocarbon or silicone pump oil that is in the air in any laboratory and difficult to avoid.

The orientational order parameter for both transitions can be determined using Equation 20. Both sets of data are shown in Figure 12. The orientational order parameter for the C 1s $\rightarrow \pi^*_{C=C}$ transition is $S_{C=C} = -0.039$, indicating a very slight orientation of the phenyl rings perpendicular to the surface. The

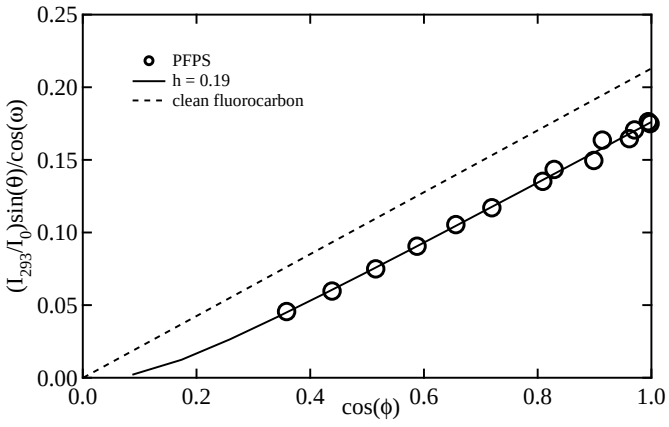

Figure 11: Data for the C 1s $\rightarrow \sigma^*_{C-F}$ transition with and without the exponential correction accounting for attenuation of the signal due to surface contamination.

fitting parameters give an order parameter of $S_{C-F} = 0$ for the C 1s $\rightarrow \sigma^*_{C-F}$ transition, indicating that there is no orientation of the $C-F$ bonds. If the side chains were to be fully extended, it would have a length of ∼1-1.4nm and the bonds would be oriented. The calculated overlayer thickness of 0.45nm indicates that the side chains are not fully extended, which is in agreement with the lack of orientation of the $C-F$ bonds.

For comparison, Figure 13 shows the NEXAFS spectra for this polymer after the post-edge data at 320eV were normalized to 1, which disregards any change in carbon atom density within the film thickness. Figure 14 shows the intensities for the two transitions of interest from the post-edge normalized spectra. By looking at the data for each transition as a function of $\cos^2(\theta)$, the density variation cannot be ignored. The C 1s $\rightarrow \pi^*_{C-F}$ transition data from the post-edge normalized spectra do not give any indication of a surface contamination layer, but is clear from the data shown in Figure 11 that the contamination is present.

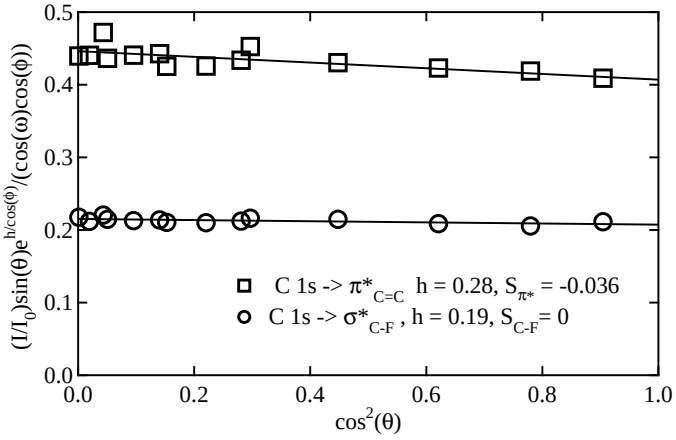

Figure 12: Intensity of the C 1s $\rightarrow \pi^*_{C=C}$ and σ^*_{C-F} transitions as a function of $\cos^2(\theta)$. The order parameters were determined using Equation 20.

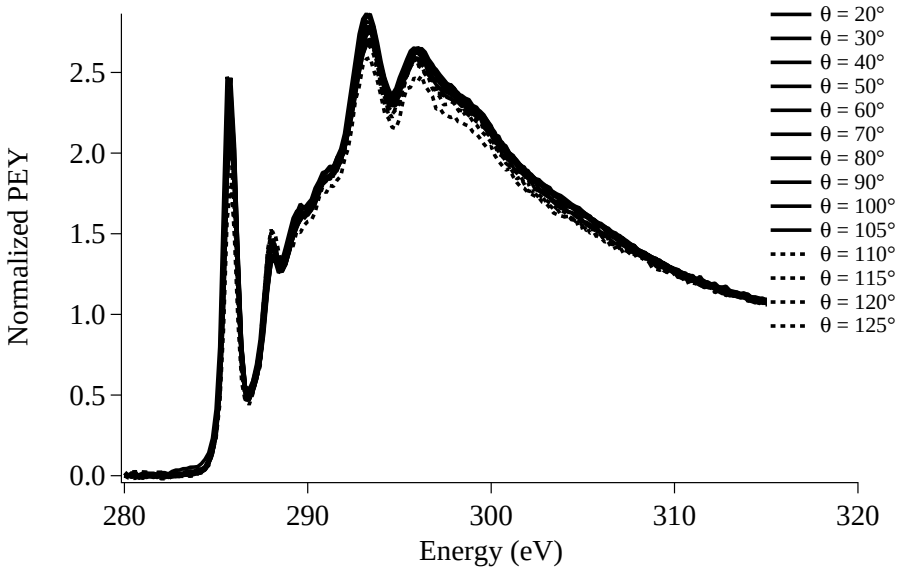

Figure 13: Post-edge normalized spectra where the difference in carbon atom density is ignored.

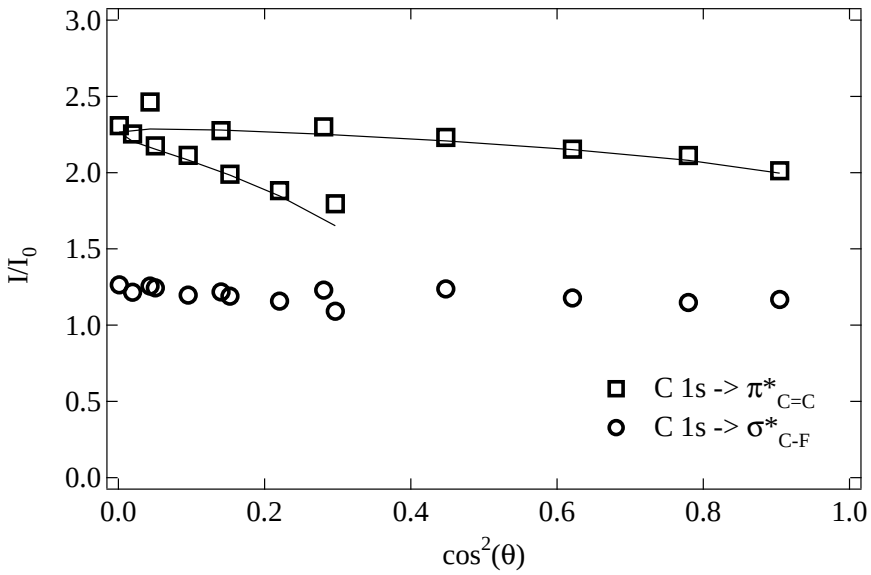

Figure 14: Intensity of the C 1s $\rightarrow \pi^*_{C=C}$ and σ^*_{C-F} transitions from the post-edge normalized spectra. Fitting the data for the C 1s $\rightarrow \pi^*_{C=C}$ yields an overlayer thickness of 0.65nm, which is larger than the value calculated using data that are not post-edge normalized.

Fitting the data for the C 1s $\rightarrow \pi^*_{C=C}$ transition gives a overlayer thickness of 0.65nm, which is significantly larger than the 0.45 nm value determined from the data that were not post-edge normalized.

As mentioned previously, Genzer et al. used fluorinated self-assembled monolayers (SAMs) to experimentally determine the EED by varying the EGB.[30] They tracked the C 1s $\rightarrow \sigma_{C-H}$ PEY signal from the methylene units connecting the perfluoroalkyl chains to the silane units that anchored the SAMs and calculated an EED of $\lambda = 2.43nm$ for an EGB of -150V. The presence of contamination is the most likely reason for the difference between the EED calculated here and that of Genzer et al. The contamination layer will have the effect of increasing the EED that they determined, which is indeed the case when the value is compared with the results here.

5 Conclusions

Depth profiling experiments using NEXAFS spectroscopy were performed on PFPE layers dip coated onto HOPG in order to experimentally determine the electron escape depth for NEXAFS using the post-edge PEY intensity, which was possible because the PFPE layer thickness was measured using variable angle ellipsometry. Fitting these data on a graph of $\frac{I_{390}}{I_0}\frac{sin(\theta)}{cos(\omega)}$ vs $\cos(\phi)$ lead to the determination of an EED of $\lambda = 1.95nm$. A new method for determining the orientational order parameter, S, was developed for data that has not been post-edge normalized. This analysis method also shows that due to the extreme surface sensitivity of NEXAFS, care must be taken to minimize sample contamination. Data from a "bare" HOPG substrate that was exposed to the air for about one minute before loading into the sample chamber and being pumped under high vacuum showed a thin layer of hydrocarbon or siloxane

contamination.

Using the post-edge values that have only been normalized by the incident beam intensity is a way to determine the number density of carbon atoms as a function of depth. This is very important since accurate fitting of the data is required to determine the thickness of surface layers. Previous work has assumed that the carbon density remains constant throughout the thickness of a polymer film, but here it is shown that this is not the case.[3]

Analysis of the post-edge intensity as well as the intensity for the C 1s $\rightarrow \pi^*_{C=C}$ transition for a polystyrene homopolymer functionalized with a perfluoroalkyl side chain shows a surface layer of lower carbon atom density than the bulk of 0.78nm thickness, which is primarily due to the surface segregation of the lower surface energy side chains. An orientational order parameter of $S_{C=C} = -0.039$ was determined, indicating that as the side chains segregate to the surface, they drag the phenyl rings with them, causing a very slight orientation of the rings perpendicular to the sample surface. The data for the C 1s $\rightarrow \sigma^*_{C-F}$ transition show that there is no preferred orientation of the side chains ($S_{C-F} = 0$), but that even though the fluorocarbon side chains have low surface energy, there is an $\sim$0.3nm thick layer of surface contamination.

6 Acknowledgements

We would like to thank Mahesh Padigala from Solvay Solexis for supplying the Fomblin Z-03. Michael Toney (SSRL), and Matthew Mate (Hitachi) are thanked for their helpful discussions. Prof. Joe Zasadzinski and his graduate student, Youngmin Jin, helped prepare the PFPE films on HOPG. Thanks to Marvin Paik and Kristin Schmidt for help with the NEXAFS measurements. Alejandro

Parra and Gila Stein helped with the ellipsometry measurements and analysis. Primary funding was provided by the NSF Graduate Research Fellowship and secondary funding by the ONR under grant number N00014-02-1-0170 and the NSF DMR Polymers Program under grant number DMR-07-04539. This work made use of central facilities at the MRL at UCSB, which is funded by the MRSEC program of the NSF under grant number DMR05-20415, and from use of the nanofabrication facilities, which is supported by the NSF-NNIN under Award No. 44771-7475. Identification of a commercial product is made only to facilitate reproducibility and to adequately describe procedure. In no case does it imply endorsement by NIST or imply that it is necessarily the best product for the procedure.

References

1. Finlay, J. A.; Callow, M. E.; Ista, L. K.; Lopez, G. P.; Callow, J. A. *Integrative and Comparative Biology* **2002,** *42,* 1116-1122.

2. Callow, J. A.; Callow, M. E.; Ista, L. K.; Lopez, G.; Chaudhury, M. K. *Journal of the Royal Society Interface* **2005,** *2,* 319-325.

3. Krishnan, S.; Ayothi, R.; Hexemer, A.; Finlay, J. A.; Sohn, K. E.; Perry, R.; Ober, C. K.; Kramer, E. J.; Callow, M. E.; Callow, J. A.; Fischer, D. A. *Langmuir* **2006,** *22,* 5075-5086.

4. Krishnan, S.; Wang, N.; Ober, C. K.; Finlay, J. A.; Callow, M. E.; Callow, J. A.; Hexemer, A.; Sohn, K. E.; Kramer, E. J.; Fischer, D. A. *Biomacromolecules* **2006,** *7,* 1449–1462.

5. DeLongchamp, D. M.; Sambasivan, S.; Fischer, D. A.; Lin, E. K.; Chang, P.; Murphy, A. R.; Frechet, J. M. J.; Subramanian, V. *Advanced Materials* **2005,** *17,* 2340.

6. Pattison, L. R.; Hexemer, A.; Kramer, E. J.; Krishnan, S.; Petroff, P. M.; Fischer, D. A. *Macromolecules* **2006,** *39,* 2225–2231.

7. DeLongchamp, D.; Kline, R. J.; Lin, E.; Fischer, D.; Richter, L.; Lucas, L.; Heeney, M.; McCulloch, I.; Northrup, J. *Advanced Materials* **2007,** *19,* 833.

8. Kline, R. J.; DeLongchamp, D. M.; Fischer, D. A.; Lin, E. K.; Heeney, M.; McCulloch, I.; Toney, M. F. *Applied Physics Letters* **2007,** *90,*.

9. Kline, R. J.; DeLongchamp, D. M.; Fischer, D. A.; Lin, E. K.; Richter, L. J.; Chabinyc, M. L.; Toney, M. F.; Heeney, M.; McCulloch, I. *Macromolecules* **2007,** *40,* 7960-7965.

10. Gurau, M. C.; Delongchamp, D. M.; Vogel, B. M.; Lin, E. K.; Fischer, D. A.; Sambasivan, S.; Richter, L. J. *Langmuir* **2007,** *23,* 834-842.

11. DeLongchamp, D. M.; Ling, M. M.; Jung, Y.; Fischer, D. A.; Roberts, M. E.; Lin, E. K.; Bao, Z. *Journal of the American Chemical Society* **2006,** *128,* 16579-16586.

12. Park, J.; Yang, R.; Hoven, C. V.; Garcia, A.; Fischer, D. A.; Nguyen, T.-Q.; Bazan, G. C.; DeLongchamp, D. M. *Advanced Materials* **2008,** *20,* 2491+.

13. Clare, A. S. *Journal of Marine Biotechnology* **1998,** *6,* 3-6.

14. Bullock, S.; Johnston, E. E.; Willson, T.; Gatenholm, P.; Wynne, K. J. *Journal of Colloid and Interface Science* **1999,** *210,* 18-36.

15. Gan, D. J.; Mueller, A.; Wooley, K. L. *Journal of Polymer Science Part A - Polymer Chemistry* **2003,** *41,* 3531-3540.

16. Youngblood, J. P.; Andruzzi, L.; Ober, C. K.; Hexemer, A.; Kramer, E. J.; Callow, J. A.; Finlay, J. A.; Callow, M. E. *Biofouling* **2003,** *19,* 91-98.

17. Schmidt, D. L.; Brady, R. F.; Lam, K.; Schmidt, D. C.; Chaudhury, M. K. *Langmuir* **2004,** *20,* 2830-2836.

18. Yebra, D.; Kiil, S.; Dam-Johansen, K. *Progress in Organic Coatings* **2004,** *50,* 75-104.

19. Lee, S.; Voros, J. *Langmuir* **2005,** *21,* 11957-11962.

20. Yagi, S.; Matsumura, Y.; Nomoto, T.; Soda, K.; Hashimoto, E.; Namatame, H.; Taniguchi, M. *Surface Science* **2007,** *601,* 4154–4157.

21. Ratner, B. D. *Surface and Interface Analysis* **1995,** *23,* 521-528.

22. Sodhi, R. N. S.; Sahi, V. P.; Mittelman, M. W. *Journal of Electron Spectroscopy and Related Phenomena* **2001,** *121,* 249-264.

23. Castner, D. G.; Ratner, B. D. *Surface Science* **2002,** *500,* 28-60.

24. Cheng, Z. Y.; Teoh, S. H. *Biomaterials* **2004,** *25,* 1991-2001.

25. Murata, H.; Chang, B. J.; Prucker, O.; Dahm, M.; Ruhe, J. *Surface Science* **2004,** *570,* 111-118.

26. Kannan, R. Y.; Salacinski, H. J.; Vara, D. S.; Odlyha, M.; Seifalian, A. M. *Journal of Biomaterials Applications* **2006,** *21,* 5-32.

27. Cheng, F.; Gamble, L. J.; Castner, D. G. *Analytical Chemistry* **2008,** *80,* 2564-2573.

28. Stöhr, J. *NEXAFS Spectroscopy;* Springer series in surface sciences Springer-Verlag: 1992.

29. Stöhr, J.; Samant, J. G. *J. Electron Spectrosc. Relat. Phenom.* **1999,** *98-99,* 187-207.

30. Genzer, J.; Kramer, E. J.; Fischer, D. A. *Journal of Applied Physics* **2002,** *92,* 7070-7079.

31. Cumpson, P. J. *Surface and Interface Analysis* **2001,** *31,* 23–34.

32. Toney, M. F.; Mate, C. M.; Leach, K. A.; Pocker, D. *Journal of Colloid and Interface Science* **2000,** *225,* 219-226.

33. Li, X.; Andruzzi, L.; Chiellini, E.; Galli, G.; Ober, C. K.; Hexemer, A.; Kramer, E. J.; Fischer, D. A. *Macromolecules* **2002,** *35,* 8078-8087.

34. Andruzzi, L.; Hexemer, A.; Li, X. F.; Ober, C. K.; Kramer, E. J.; Galli, G.; Chiellini, E.; Fischer, D. A. *Langmuir* **2004,** *20,* 10498–10506.

35. Toomey, R.; Mays, J.; Tirrell, M. *Macromolecules* **2004,** *37,* 905-911.

36. Stroumpoulis, D.; Parra, A.; Tirrell, M. *AICHE Journal* **2006,** *52,* 2931-2937.

37. Starkweather, H. W. *Journal of Polymer Science Part B - Polymer Physics* **1982,** *20,* 2159-2161.

Table of Contents

Depth Profiling the Near Surface of Polymer Films Using NEXAFS Spectroscopy

Karen E. Sohn, Michael D. Dimitriou, Jan Genzer, Daniel A. Fischer, Craig J. Hawker, and Edward J. Kramer

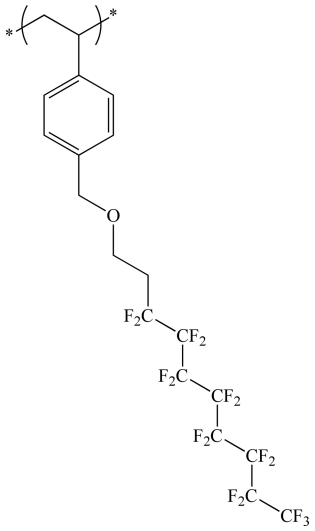

(a)

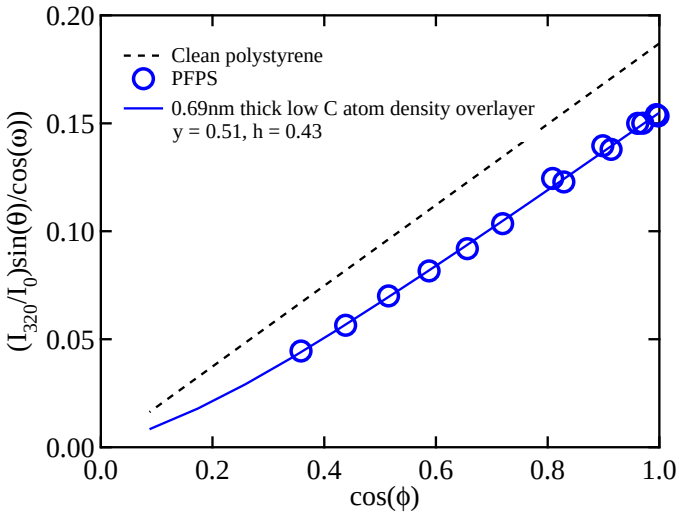

(b)